IEEE Access
Multidisciplinary | Rapid Review | Open Access Journal

Received May 21, 2019, accepted June 30, 2019, date of publication July 3, 2019, date of current version July 23, 2019.

Digital Object Identifier 10.1109/ACCESS.2019.2926629

Analysis on Integrated Energy System Cascading Failures Considering Interaction of Coupled Heating and Power Networks

YI PAN[1], FEI MEI[2], CHENG ZHOU[1], TIAN SHI[1], AND JIANYONG ZHENG[1]
[1]School of Electrical Engineering, Southeast University, Nanjing 210096, China
[2]College of Energy and Electrical Engineering, Hohai University, Nanjing 211100, China

Corresponding author: Jianyong Zheng (zhengjy_seu@163.com)

This work was supported in part by the National Key R&D Program of China under Grant 2018YFB0905002.

ABSTRACT As the coupling and integration of multi-energy flow in the integrated energy system (IES) deepen increasingly, the cascading failure will develop across different energy systems more easily and widely through the energy hub (EH). And it brings great challenges to the security and reliability of IES. The defects of the present cascading failure model of IES have been summarized, and a novel search strategy of fault chains in IES combined heating and power network was proposed in this paper. First, the initial risk assessment index of each energy branch is proposed to form the initial fault sets. Then, combined heat and power control (CHPC) strategies are introduced to deal with the branch overload conditions during the cascading failure. What is more, in order to reduce the workload and overcome the limitation of present methods, we analyzed the relevance of the branches to be predicted by using the kernel fuzzy C-means (KFCM) clustering algorithm and select the branches with the highest value of relevance as the subsequent failure. Based on the predicted fault chain, vulnerability analysis is presented to locate critical component and find out the correlation between cascading outages. The comprehensive evaluation index is also established to effectively evaluate the impact severity of cascading failure. Finally, the case studies are carried out on the combined heating and power systems to demonstrate the effectiveness of the proposed method.

INDEX TERMS Integrated energy system, cascading failure, energy hub, combined heating and power network, risk assessment, vulnerability analysis.

I. INTRODUCTION

As the main carrier of the energy internet, the integrated energy system (IES) plays an important role in promoting the energy comprehensive utilization efficiency and meeting the integrated energy demand [1], [2]. There exist multiple coupling forms in IES, such as heat-power coupling, gas-power coupling, and heat-power-gas coupling, which can realize the conversion, complementary and dispatch between different energy systems through the energy hub (EH) [3].

The deeper coupling between different energy systems makes the interaction mechanism of them more complex. A disturbance or a failure in one system may influence another system through the coupling component, which leads to higher probability and lager scale of cascading failures [4]–[6]. Heat and power are the most common end-user energy demands, the coupling between these two energy systems is tight and fault development modes are complex, so studying the propagation and evolution characteristics of the cascading failure between heating and power systems is of great significance for identifying the vulnerable component and preventing the development of cascading failures. Energy hub is the key to combine the district heating system and power system [7], it usually consists of various thermo-electric coupling components, such as combined heat and power (CHP) units, electric boilers (EB), heat pumps (HP), circulating pumps (CP) and so on.

At present, there are many researches on the theory and modeling methods of cascading failures in power systems, mainly focusing on the simulation of cascading failures, critical fault path searching and vulnerable lines identification. In Reference [8], a risk assessment model of power system cascading failures is presented based on the fault chain. A Markovian tree searching method is adopted to

The associate editor coordinating the review of this manuscript and approving it for publication was Arup Kumar Goswami.

predict the multi-timescale cascading outages in Reference [9]. To quickly predict the distribution of blackout sizes, the branching processes are applied to simulated cascading data in Reference [10]. However, the dynamic interaction process of different energy systems during cascading failures is ignored in its existing evolution models. In addition, association between cascading outage events and influence of outage sequences are not well analyzed. Considering the effects of gas system, a model of cascading failures of power system integrated natural gas fired generators is established in Reference [11], while it only covers one-way propagation of the failures between gas and power systems. In Reference [12], the interaction characteristics of district heating and power systems under different failure modes are analyzed based on quasi-steady energy flow. In Reference [13], the non-sequential Monte Carlo method is applied to the risk assessment for IES. Although the above researches consider the interaction effects of different energy systems, the efforts focused on the modeling and analysis of the complete fault chain across different energy systems is still insufficient.

The bidirectional energy flow of the coupled heating and power systems promotes the bidirectional propagation of cascading failures [14], [15]. Therefore, how to effectively analysis the interaction characteristics between heating and power network, simulate the development process of the cascading failure and locate the vulnerable component for the IES are urgent problems to be solved [16]. In Reference [17], a static sensitivity analysis of the integrated power and gas system is proposed based on unified power flow model. The similar idea can be learned to promote further extension to the integrated power and heating system or the integrated power, gas and heating systems. What's more, control strategies play an important role in the development of cascading failures of IES [18]–[20]. By adjusting the power and heat generation of EHs with the proper control strategies, the imbalance or the branch overload can be decreased, so as to improve safety operation margin and reduce the probability of cascading failures in IES [21], [22].

This paper proposed a simulation model of the cascading failure in IES. Focusing on the interaction effects of coupled heating and power network, the cascading outage events for different initial outages will be simulated to form the complete fault chain. Based on fault chains, the correlation between cascading outage events and influence of outage sequences are well analyzed. The cascading failure model can be divided into four main steps: 1) selection of the initial fault sets; 2) application of the combined heat and power control strategies; 3) prediction of the subsequent random failure; 4) comprehensive assessment of the fault chain. This model applies the control strategies to both power network side and heating network side to deal with the overload of the power lines or the pipelines caused by the initial failure. What's more, we combined the state transition evaluation and the implicit failure probability as the relevance index, analyzed the relevance of the branches to be predicted by using Kernel Fuzzy C-means (KFCM) clustering algorithm and selected the branches with the highest value of relevance as the subsequent failure. Finally, the case studies are carried out on the combined heating and power systems to demonstrate the effectiveness of the proposed method. Based on the simulated fault chain, the vulnerable component of IES can be furthermore located, which contributes to formulating the prevention and blocking strategies for cascading failures.

II. MODEL FOR THE COUPLED HEATING AND POWER NETWORKS

A. SYSTEM STRUCTURE

This paper focus on the IES combined district heating and power network, in which EHS are responsible for the main supply of power and thermal load of the IES, especially when the whole system is isolated from external systems. The typical structure of the IES combined district heating and power network is shown in Fig. 1.

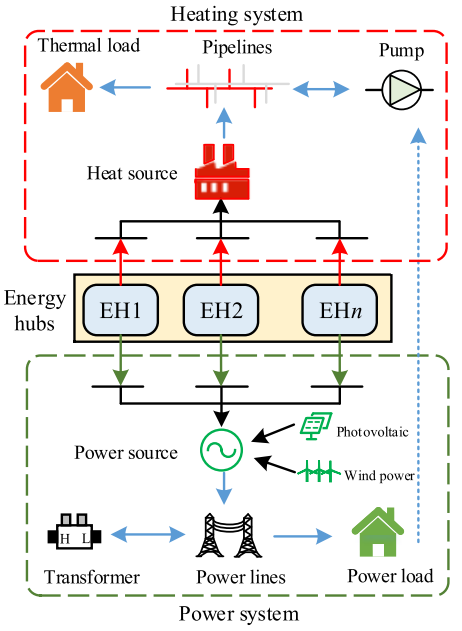

FIGURE 1. Structure of IES combined heating and power networks.

The heating network consists of the heat source, supply and return pipes that deliver hot water, heat exchange station, circulation pump and the thermal load. The water is heated in the heat source side, such as the energy hub and heat plants, and is delivered to the load side through the pipelines, so as to meet the thermal demand. The circulation pumps are potentially critical devices, which drive the water flow in the heating network. Due to the power consumption during the operation of pumps, it can be equivalent to part of the power load. The power network is composed of the power source, power lines that deliver electricity, transformers that connect networks with different voltage levels, and the power load. Multiple power source forms are included to supply the power load, such as the power generation of EH, photovoltaic

generation, wind power generation and so on. The heating and power network are coupled through multiple EHs, which has high flexibility to adjust the operation state of the IES.

According to the interaction mode between the IES power network and the external power system, the IES operation can be divided into the two modes: grid-connected mode and islanded mode. In grid-connected mode, one EH is selected as the slack node of the heating network, which is defined to supply the heat difference between the total system loads and the specified heat output. The connection point to the external power system is selected as the power slack, so the power supply fluctuations in the IES can be balanced through the external power grid, which has stronger scheduling ability, and this results in weaker coupling between the heating and power networks. While in islanded mode, the power and heat slack nodes are both selected from the different EHs, which means that the operation sate of the whole IES should be balanced only by EHs, which results in the stronger coupling between two energy networks, and increases the probability and complexity of the IES cascading failures. So it is meaningful to focus on the islanded mode of IES in this paper.

B. POWER SYSTEM MODEL

The power network usually adopts the traditional AC power flow model [23], the state variables to be solved include the node voltage, phase angle, real and reactive power injections. Considering that the development of the power-side cascading failure is mainly related to the power flow transferring of the power lines, so the power system in this paper is modeled by using the DC power flow [24] to highlight the impact of the power flow on the failure evolution process, which contributes to decreasing the complexity of the model and improve the solution efficiency. The model of DC power flow can be described as (1):

$$\boldsymbol{P} = \boldsymbol{B_0\theta} \tag{1}$$

where $\boldsymbol{B}_0$ represents the susceptance matrix of the power branch, and the power flow in the power line can be calculated as (2):

$$P_{ij} = \frac{(\theta_i - \theta_j)}{x_{ij}} \tag{2}$$

where x_{ij} is the line reactance, P_{ij} is the real power in the branch i-j, θ_i and θ_j represent the voltage angles of the node i and j.

C. HEATING SYSTEM MODEL

According to the basic operation mechanism of the district heating network, it can be modeled combining a hydraulic model and a thermal model [14]. Similar to the Kirchhoff's current law (KCL) and Kirchhoff's voltage law (KVL) in power system, the hydraulic model can be expressed as (3), the state variables to be solved in the hydraulic model are: mass flow rates and the head pressure loss.

$$\begin{cases} \boldsymbol{Am} + \boldsymbol{m_q} = 0 \\ \boldsymbol{Bh}_f = \boldsymbol{BKm}\,|\boldsymbol{m}| = 0 \end{cases} \tag{3}$$

where $\boldsymbol{A}$ is the node-branch incidence matrix, $\boldsymbol{B}$ is the Branch-loop incidence matrix, $\boldsymbol{K}$ is the resistance coefficient matrix of the pipe, and $\boldsymbol{h}_f$ is the vector of head pressure loss. $\boldsymbol{m}$ represents the vector of mass flow rates within each pipe, and $\boldsymbol{m}_q$ represents the vector of mass flow rates injected from the load node or the source node.

The thermal model is used to calculate the water temperature at each node, which is calculated as (4). It consists of the equation of the temperature loss along the pipe, the equation of the water mixture and the equation of the heat power transferring.

$$\begin{cases} T_{end} = (T_{start} - T_a)\, e^{-\zeta L/m} + T_a \\ \left(\sum \boldsymbol{m}_{out}\right) T_{out} = \sum (\boldsymbol{m}_{in} T_{in}) \\ \boldsymbol{H}_{ex} = C_p \boldsymbol{m}_q\, (T_s - T_r) \end{cases} \tag{4}$$

where T_{start} and T_{end} represent the start and end node of the pipe, T_a is the ambient temperature, L is the length of the pipe, and ζ is the proportional coefficient related to parameters of the pipe. $\boldsymbol{m}_{in}$ and $\boldsymbol{m}_{out}$ respectively represent the vector of mass flow rates injected at the node and leaving the node. T_{in} is the water temperature at the end of the incoming pipe and the T_{out} is the mixture temperature of the node. $\boldsymbol{H}_{ex}$ is the vector of heat power consumed by load or supplied by heat source. C_p is the specific heat of water. T_s and T_r indicate the supply and return water temperature at each node.

D. ENERGY HUB MODEL

EHs are responsible for connecting the heating system and power system, which ensure the bidirectional energy flow between two systems. Fig. 2 shows the typical structure of a EH.

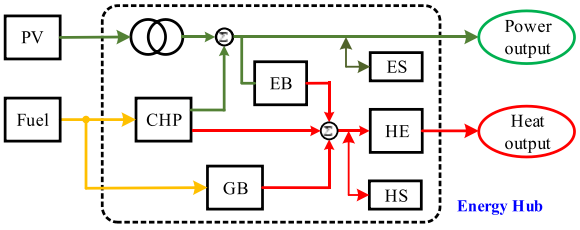

FIGURE 2. The structure of one typical energy hub.

In this paper, the EH is mainly composed of multiple coupling components: the combined heat and power (CHP) unit that generates power and heat simultaneously, electric boilers (EB) that transfers electricity into heat, gas boilers (GB) that generate power by consuming natural gas, heat exchangers (HE), electricity storage (ES), heat storage (HE), and the photovoltaic generation system (PV). The fuel of the EH is natural gas, and it is assumed that the supply of natural gas is sufficient and continuous in this paper. The output

characteristics of the EH are determined to the configuration and operation strategies of the coupling components inside. In order to ensure the safe and economical operation of IES, EHs are required to play more active role in system operation by taking advantage of the its flexibility. According to the adjustability of thermoelectric ratio of the CHP unit, the EH can be divided into two models with different flexibility.

For the CHP unit with a fixed thermoelectric ratio c_{am}, the output preferentially meets the thermal demand, which limits the flexibility of the power generation. The power output P_{am} and heat output Q_{am} of the CHP with a fixed thermoelectric ratio should meet the constraints (5):

$$\frac{Q_{am}}{P_{am}} = c_{am} \tag{5}$$

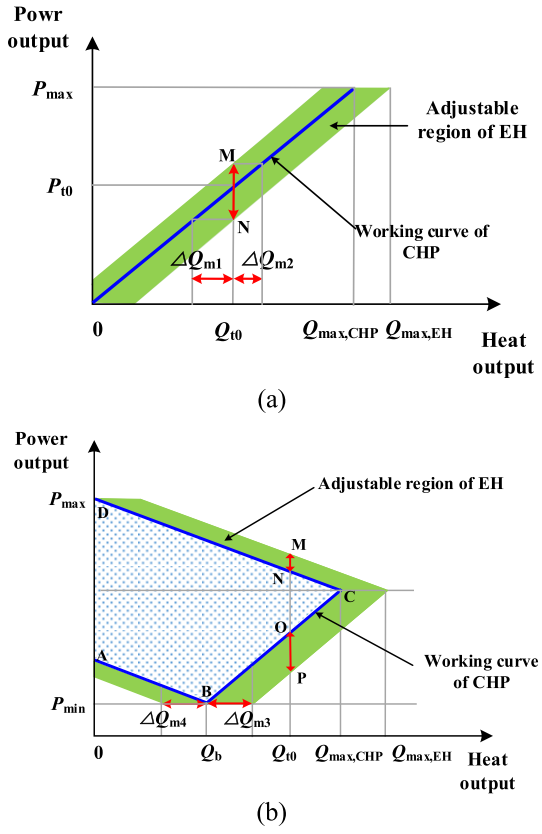

FIGURE 3. (a) Output curve of the EH with the fixed-thermoelectric ratio CHP. (b) Output curve of the EH with the variable-thermoelectric ratio CHP.

Fig. 3 (a) shows the output characteristics of the EH with the fixed thermoelectric ratio CHP. When running at the t_0 point, the CHP outputs the fixed heat Q_{t0}. Due to the coordination and complementarity of coupling components in EH, the EH can obtain additional adjustable margin of heat generation (ΔQ_{m1} plus ΔQ_{m2}), as well as the additional flexible range of power generation, which is expressed as the line segment "*MN*". Compared with the single CHP unit, the EH with multiple coupling units inside can generate heat and power in a more flexible operation region. The output of the EH with the fixed thermoelectric ratio CHP should meet the constraints (6):

$$\begin{cases} \max\left\{\left(Q-\Delta Q_{m1}\right)/c_{am}, 0\right\} \\ \quad \le P \le \min\left\{\left(\Delta Q_{m2}+Q\right)/c_{am}, P_{max}\right\} \\ 0 \le Q \le Q_{max,EH} \end{cases} \tag{6}$$

where ΔQ_{m2} and ΔQ_{m1} represent the upper and lower parts of the adjustable margin of EH heat generation. $Q_{max,EH}$ and P_{max} are the maximum heat and power output of the EH.

Containing the CHP with the variable thermoelectric ratio, the operation region of the EH becomes more flexible. The output curve of the EH is presented in Fig. 3 (b). When the thermal demand is Q_{t0}, the CHP with a variable thermoelectric ratio can supply the power in the range of the line segment "ON", and there exists additional adjustable margin (ΔQ_{m3} plus ΔQ_{m4}) of heat generation in the EH, where the ΔQ_{m3} can be regarded as the extra heat supply generated from the EB, GB and HS, the ΔQ_{m4} can be regarded as the heat supplied for heat storage. At the same time, the power output range of the EH becomes the line segment "MP", adding the extra margin ("*MN*" plus "*OP*") for the flexible dispatching. The output of the EH with the variable-thermoelectric ratio CHP should meet the constraints (7):

$$\begin{cases} \min\left\{\begin{array}{l} P_{min}+\left(Q-Q_b-\Delta Q_{m3}\right)/c_m, P_{min}, P_{min}+ \\ \left(Q_b-Q\right)/c_a-\Delta Q_{m4}/c_a \end{array}\right\} \\ \le P \le \max\left\{P_{max}, P_{max}-\left(Q-\Delta Q_{m3}\right)/c_b\right\} \\ 0 \le Q \le Q_{max,EH} \end{cases} \tag{7}$$

where P_{min} and Q_b represent the minimum power and heat generation of the EH at the running point *B*. P_{max} is the maximum power generation of the EH at the running point D. c_m, c_a and c_b are the elastic coefficients of the power and heat output under different running conditions [25].

E. SOLUTION OF THE MULTI-ENERGY FLOW

In this paper, the multi-energy flow of the coupled heating and power network is solved by the decomposed method, which has the advantages of simple programming and fast calculation. In the calculation process, the independent power system and heating system are calculated sequentially and linked through EHs. The sequential calculation procedure will keep iterating until the solution converges to an acceptable tolerance. The solution process is as follows:

Step1. Analysis the topology of the coupled heating and power network, set specified parameters for each node and branch, and initialize the unknown state variables of the whole system.

Step2. For the islanded mode of IES, two EHs with sufficient capacity and high flexibility will be selected as the power slack node and the heat slack node, other EHs are given as the PV node, PQ node, or the heat source node.

Step3. According to (3) and (4), the forward-backward sweep method [26] is used to independently calculate the state variables in the heating network, such as the node pressure, temperature and the pipe mass flow rates.

Step4. Based on the calculation results of the heating network, update the power generation and power load of each node in the power network with the constraints of EH. Then calculate the power flow of each power line and the power generation of the power slack node according to (1)(2).

Step5. Take the sate calculation results of the power network as the specified parameters to update the sate variables of the heating network.

Step6. The sequential procedure from Step4 to Step5 is iterated until the solution converges to an acceptable tolerance, then output the sate variables of the power-heat flow.

III. CASCADING FAILURE MODEL FOR THE INTEGRATED ENERGY SYSTEM

A. EVOLUTION PROCESS OF CASCADING FAILURE

Security is the basis of the normal operation of IES, which is usually affected by various failures during the operation. Different from the failure development mode in traditional power system, the failures occur in IES will convey dynamically between the heating and power network due to the variation of the EH output. For example, if there exists an initial failure in the power network of IES, the EH, which is at the slack node, will respond to the failure to balance the power flow. This may lead to the variation of the heat output of the EH and the variation degree mainly depends on the flexibility of the EH. As a result, the sate variables of the heating network may change, causing the heating output variation of the EH at the heating slack node. The variation can be regarded as a new disturbance in heating network, which can in turn influence the power network. Thus, the two systems interact with each other until the final stable condition is reached. During the interaction process, the multi-energy flow may exceed the limits of each branch, which has the possibility to cause the new failures, such as the power line outage and pipe leakage, so as to result in the development of the cascading failures. In conclusion, the propagation of the failures is bidirectional in IES, which leading to the complicated evolution process of cascading failures.

Referring to the traditional development process of cascading failures in power system [27], [28], the whole evolution process of the cascading failures in IES combined the heating and power network can be divided into four main stages.

Stage1. Pre-failure stage. In this stage, the power system of IES is operating in the normal condition with low security margin, which is close to the boundary conditions of the protection device action and coordinated management implementation.

Stage2. Initial failure stage. In this stage, the failure and outage of single or multiple components is the direct cause of the cascading failure. For example, the serious overload of some power lines will trigger the action of the protection device to cause the line outage, while the leakage and aging of the pipelines are usually managed by isolating the portion of pipeline where the failure occurs.

Stage3. Failure spreading stage. After the outage of some power lines and pipelines due to the protection device action or the coordinated management, the multi-energy flow transition may occur in the IES, which leads to the development of cascading failures. In power network of IES, the overload of power lines and the random failure are main factors that promote the cascading failure. Compared with the power system, the heat transmission speed is lower, and the security margin of operation is higher due to the thermal inertia and heat storage characteristics of the heating network. As a result, the failures and pipe outages requires the state accumulation with a long-term scale, and the real-time requirements for fault removal are relatively low in the heating network. So, the coordinated optimization control strategies will be applied to deal with the malfunctions occur in heating network.

Stage4. Fast outage stage. In this stage, a large number of components outages occur in short-term, leading to the system splitting, power outage and the heat supply interruption.

B. SIMULATION FLOW OF CASCADING FAILRUE

The model of cascading failure proposed in this paper mainly considers the impact of the energy flow transfer on the failure evolution process. The simulation of cascading failures in IES is realized by searching and predicting the fault chains. The flow chart is shown in Fig. 4, and the concrete process is summarized as follows:

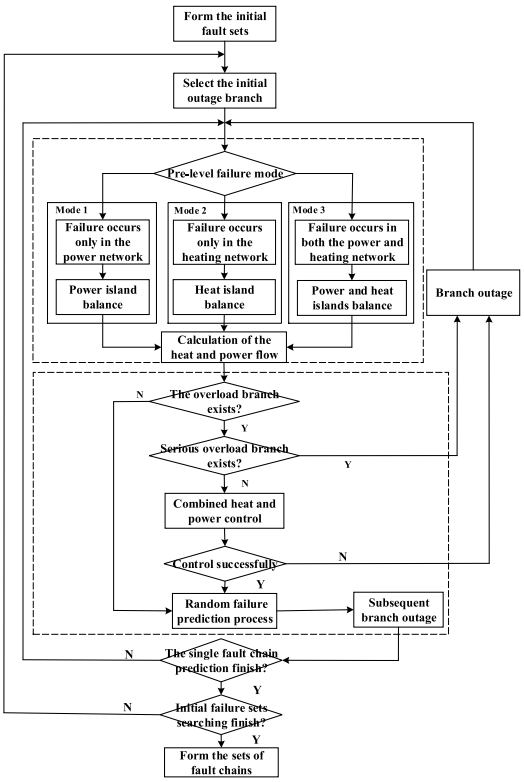

FIGURE 4. Flow chart of the cascading failure simulation.

Step 1. Firstly, based on the calculation results of the initial risk indicators established in the next section, the power lines and pipelines with high risk value are screened within the threshold range to form the initial fault sets.

Step 2. Randomly select the branch from the initial fault sets as the occurred initial failure, and isolate the corresponding power line or pipeline, which is regarded as the first outage component.

Step 3. Determine the pre-level failure mode.

Mode 1: The failure only occurs in the power network and the corresponding power line is outage.

Mode 2: The failure only occurs in the heating network and the corresponding pipeline is outage.

Mode 3: The failure occurs both in the two systems.

Due to the influence of the pre-level failure, there may exist energy islands in the power and heating network. For power islands, it is necessary to formulate control strategies of the power generation and electricity load in the island to ensure the power balance. If the reserve capacity in the power island is sufficient, the output of the generator at each node will be proportionally increased according to the residual generation capacity. If the reserve capacity of the power island is insufficient, the generator at each node will output at the maximum value, and the electricity load should be reduced in proportion to the power shortage [11]. For the heat islands, the heat balance in the island can be achieved by adjusting the heat generation and the thermal load with the similar control strategies to the power island.

Step 4. If the new energy island occurs in the power or heating network, the energy balance of the island will be performed according to the control strategies described in Step3. Otherwise, skip to the Step 5 directly.

Step 5. Calculate the multi-energy flow. If there exists the overload in the power line or pipeline, the Step6 will be continued, otherwise skip to the Step7 directly.

Step 6. Determine the position of the overload, and formulate proper coordinated control strategies according the position and severity of overload. Assume that the max load rate of the power line is $\beta_{L,max}$, if the load rate of the power line meets the condition: $\beta_L \geq 1.5\beta_{L,max}$, it can be regarded as the serious overload branch; If the condition $\beta_{L,max} \leq \beta_L 1.5\beta_{L,max}$ is met, it can be regarded as the normal overload branch. If the serious overload occurs in the power line, the protection device will act to isolate the corresponding branch, then the current outage event prediction process is finished and we go back to Step 3. When the normal overload occurs in the power network or the pipeline overload occurs in the heating network, the combined heat and power control strategy, which is modeled in the next section, will be applied to decreasing the overload conditions. If the control strategy works, the current outage event prediction process is finished, and we skip to the next Step. While if the control strategy does not work, the overload branch will be taken as the subsequent outage branch, then we go back to Step 3.

Step 7. The random failure prediction process begins. In this step, there exists no overload branch and the random failure of the branch becomes the main factor to promote the development of cascading failures. By combining the state transition evaluation and the implicit failure probability as the relevance indictor, the relevance of the branches to be predicted will be analyzed with KFCM clustering algorithm and the branches with the highest value of relevance will be selected as the subsequent outage.

Step 8. Determine whether the prediction process of the single fault chain is completed. If the ending condition is met, the prediction process will be finished and a complete fault chain corresponding to the initial fault will be formed. The prediction ending condition for single fault chain includes: 1) The outages in the current fault chain cause the multi-energy flow unable to converge; 2) The total load loss ratio exceeds the upper limits; 3) The number of the outages included in the fault chain has reached specified maximum.

Step 9. The procedure of the fault chain prediction will keep performing until all failures in the initial fault sets are searched.

C. MODEL CONSTRUCTION FOR CASCADING FAILURE

1) MODEL FOR THE INITIAL FAILURE SELECTION

The initial comprehensive risk assessment indicator of the coupled heating and power network can be defined as (8):

$$R_{Li} = P_{Li,0} \times D_{Li,0} \times W_{Li,0} \times E_{Li,0} \tag{8}$$

where the indicator component $P_{Li,0}$, $D_{Li,0}$, $W_{Li,0}$ and $E_{Li,0}$ separately represent the fault probability, initial load rate, initial energy flow ratio and the outage influence of each branch. The calculation expression of each indicator component is described as (9):

$$\begin{cases} P^k_{Li,0} = L_{i,k} / \left(\sum_{j \in \Omega_k} L_{j,k} \right) \\ D^k_{Li,0} = F^k_{Li,0} / F^k_{Li,\max} \\ W^k_{Li,0} = F^k_{Li,0} / \left(\sum_{j \in \Omega_k} F^k_{Lj,0} \right) \\ E^k_{Li,0} = \sum_{L_j \in \Omega_1 + \Omega_2, j \neq i} \Delta F^k_{Lj} / F^k_{Lj,0} \end{cases} \tag{9}$$

where $L_{i,k}$ is the length of the i-th branch. Ω_k is the set of power lines and pipelines. If the k is set as 1, Ω_k will represent the sets of the power lines, if the k is set as 2, Ω_k will represent the sets of the pipelines; $F^k_{Li,\max}$ is the upper limitation of the power flow or mass flow rate in the i-th branch, $F^k_{Li,0}$ is the power flow or mass flow rate in the i-th branch before the initial failure occurs, and ΔF_{Lj} is the variation of power flow or mass flow rate in the j-th branch after the initial outage L_i.

The initial risk values of power lines and pipelines are calculated according to (8) and (9), and the branches with high risk can be further selected to form the initial fault sets.

2) COMBINED HEAT AND POWER CONTROL MODEL

The heating network and power network are deeply coupled through EHs, the control strategy performed on one system may influence the flow distribution of another system, even causing the new disturbance. So, the control strategies

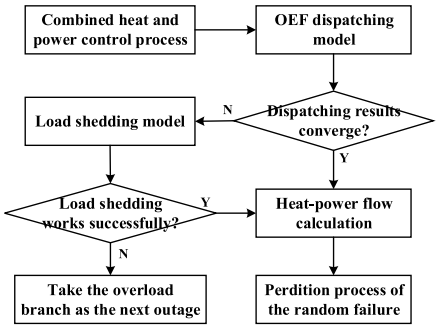

FIGURE 5. Model structure of the combined heat and power control strategies.

should take the restrictions of both power network and heating network into account and the resources for dispatching on both sides should be fully excavated, so as to realize the co-controlling for the integrated heating and power network. Fig. 5 shows the model structure of the combined heat and power control strategies (CHPC), which consists of the optimal energy flow (OEF) dispatching model and the load shedding model.

(1) The dispatching model of the optimal energy flow

Aiming at obtaining the optimal energy flow with low management costs under the premise of ensuring the security operation of IES, a dispatching model is established in this paper, which is driven by the minimizing the total operation costs of IES.

$$\min Cost\ (\boldsymbol{x}_e, \boldsymbol{x}_h, \boldsymbol{x}_c) \tag{10}$$

where the vector $\boldsymbol{x}_e, \boldsymbol{x}_h$ and $\boldsymbol{x}_c$ represent the independent variables to be optimized in the power network, heating network and the EH, and they can be further expressed as:

$$\begin{aligned} x_e &= \left[P_{eh,1}, P_{eh,2}, \ldots, P_{eh,m}, P_{g,1}, \ldots P_{g,n}\right] \\ x_h &= \left[Q_{eh,1}, Q_{eh,2}, \ldots, Q_{eh,m}, T_{s,1}, \ldots, T_{s,m}\right] \\ x_c &= \left[x_{c,1}, x_{c,2}, \ldots, x_{c,m}\right] \end{aligned} \tag{11}$$

where m is the number of EHs except the power and heat slack nodes. n is the number of the generators in the power network. $P_{eh,i}$ is the power generation of the i-th EH except the power slack node, and $P_{g,j}$ is the power output of the j-th generator. $Q_{eh,i}$ represents the heat generation of the i-the EH, and $T_{s,j}$ is the supply temperature of the j-th EH. $\boldsymbol{x}_{c,i}$ is the vector of the output of coupling components in the i-th EH.

The calculation method of the operation costs of IES can be further expressed as (12), which consists of the operation and maintenance costs f_{om} of each equipment, the fuel cost f_{fluel} of EH, the cost f_{loss} of the power and heat loss in the IES network.

$$Cost = \sum_{i \in \boldsymbol{\Pi}_1} f_{om,i}\left(\boldsymbol{x}_e, \boldsymbol{x}_h, \boldsymbol{x}_c\right) + f_{fuel}\left(\boldsymbol{x}_c\right) + f_{loss}\left(\boldsymbol{x}_e, \boldsymbol{x}_h\right) \tag{12}$$

where Π_1 represents the sets of the equipment working in IES, such as generators, circulating pumps, and the coupling components of each EH.

The constraints of the dispatching model mainly include: The equation constraints (13), which are based on (1)-(4), including the power balance, heat balance, and the energy conversion balance of each EH; The output constraints (14) of each power or heat generation equipment; The inequality constraints (15) of each EH considering the dispatching flexibility, which are based on (6)(7); Operation constraints (16) of the power network and heating network, such as the power flow range constraints, voltage range constraints, supply temperatures range constraints, and the mass flow rate range constraints.

$$E\left(\boldsymbol{x}_e\right) = 0, \quad H\left(\boldsymbol{x}_h\right) = 0, \ C\left(\boldsymbol{x}_c\right) = 0 \tag{13}$$

$$\underline{P_{e,i}} \le x_{e,i} \le \overline{P_{e,i}}, \quad \underline{Q_{h,i}} \le x_{h,i} \le \overline{Q_{h,i}}, \ \underline{P_{c,i}} \le x_{c,i} \le \overline{P_{c,i}} \tag{14}$$

$$EH\left(\boldsymbol{x}_e, \boldsymbol{x}_h, \boldsymbol{x}_c\right) \le 0 \tag{15}$$

$$EN\left(\boldsymbol{x}_e\right) \le 0, \quad HN\left(\boldsymbol{x}_h\right) \le 0 \tag{16}$$

(2) Load shedding model

Considering the time limitation of the dispatching in abnormal conditions, the load shedding strategy will be applied to dealing with the abnormal operating condition if the OEF dispatching model cannot converge.

The load shedding model is driven by minimizing the total load shedding under the premise of ensuring the security operation of IES, which can be expressed as (17):

$$\min f\ (\alpha, \beta) = \min \left\{ \sum_{i \in \Omega_e} \alpha_i P_{L_i} + \sum_{j \in \Omega_h} \beta_j Q_{L_j} \right\} \tag{17}$$

where α and β respectively represent the power load shedding ratio and the thermal shedding ratio. Ω_e is the sets of the adjustable power loads, Ω_h is the sets of the adjustable thermal loads.

The constraints of the load shedding model mainly include: the power and thermal load shedding constraints (18)(19), where the $\Delta P_{k,max}$ and $\Delta Q_{k,max}$ respectively represent the maximum value of the power and thermal load shedding; Overload margin constraints (20) after the load shedding. Other constraints (21), which consist of both equality and inequality constraints described in (13)-(16), while the variables to be optimized should be replaced with the load shedding ratio.

$$\Delta P_k \le \Delta P_{k,\max} \tag{18}$$

$$\Delta Q_k \le \Delta Q_{k,\max} \tag{19}$$

$$\phi\left(\Delta P_k, \Delta P_k\right) \ge \varepsilon \tag{20}$$

$$\Phi\left(\alpha, \beta\right) = 0, \quad \varphi\left(\alpha, \beta\right) \le 0 \tag{21}$$

3) PREDICTION MODEL OF THE RANDOM FAILURE

The prediction process of the random failure is modeled by combining the state transition evaluation and the implicit failure probability as the relevance index.

The state transition evaluation indexes include the branch load rate λ, the variation rate μ of multi-energy flow, and

the impact factor γ of the branch outage. Assume that the m-th outage component of the fault chain is the branch l_i, and l_k is one of the branches to be predicted for the subsequent outage.

The load rate index reflects the mean load rate of the branch before and after the m-th outage occurs, and it can be calculated according to (22):

$$\lambda_{k(m+1)} = \left| \frac{f_k^m + f_k^{m+1}}{2f_{k,max}} \right| \tag{22}$$

where f_k^m and f_k^{m+1} respectively represent the power flow or mass flow rate in the branches before and after the m-th outage occurs. $f_{k,max}$ is the upper limitation of the power flow in the power line or the mass flow rate in the pipeline.

The variation rate of multi-energy flow can be expressed as (23), which reflects the variation of the power flow and the mass flow rate due to the effect of the m-th outage.

$$\mu_{k(m+1)} = \begin{cases} \left| \dfrac{f_k^{m+1} - f_k^m}{f_k^m} \right| & k \in \Psi_1 \\ \dfrac{1}{2}\left(\left| \dfrac{f_k^{m+1} - f_k^m}{f_k^m} \right| + \left| \dfrac{T_k^{m+1} - T_k^m}{T_k^m} \right| \right) & k \in \Psi_2 \end{cases} \tag{23}$$

where Ψ_1 is the set of power lines to be predicted, and Ψ_2 is the set of pipelines to be predicted. T_k^m and T_k^{m+1} respectively represent the water temperature in the pipelines before and after the m-th outage.

The impact factor of the branch outage is calculated by (24), indicating the influence degree of the former outage.

$$\gamma_{k(m+1)} = \left| \frac{f_k^{m+1} - f_k^m}{f_i^m} \right| \tag{24}$$

where f_I^m is the power flow or mass flow rate in the branch l_i before its outage.

The implicit failure mainly occurs in the power network, which is related to the power flow in the branch after the former outage. While the probability of the implicit failure occurs in the heating network is set as a constant p_0 with low value in this paper. The implicit failure probability of the branch can be expressed as (25).

$$h_{k(m+1)} = \begin{cases} p(f_k^{m+1}) & k \in \Psi_1 \\ p_0 & k \in \Psi_2 \end{cases} \tag{25}$$

where $p(fm + 1\ k)$ is the probability of the implicit failure occurs in the k-th power line, which can be calculated as:

$$p(f_k^{m+1}) = \begin{cases} 0.05 & f_k^{m+1} < f_{HF} \\ \dfrac{2f_k^{m+1} - f_{HF}}{2f_{set} - f_{HF}} & f_{HF} < f_k^{m+1} < f_{set} \\ 1 & f_k^{m+1} > f_{set} \end{cases} \tag{26}$$

where f_{set} is the maximum power flow $f_{k,max}$ in the power line, and $f_{HF} = 0.75 f_{k,max}$.

The four indictors can be further combined to form the relevance vector corresponding to the m-th outage branch: $R_k^{m+1} = \left[\lambda_{k(m+1)}, \mu_{k(m+1)}, \gamma_{k(m+1)}, h_{k(m+1)}\right]$.

The comprehensive relevance indictor for outage prediction is defined as (27):

$$C_{k,m+1} = \alpha_{k(m+1)}\beta_{k(m+1)}\gamma_{k(m+1)} + h_{k(m+1)} \tag{27}$$

Calculate the relevance vector of the branches to be predicted and cluster the vectors by using KFCM algorithm. Then select the sets of branches with the highest comprehensive relevance of their clustering center as the subsequent outage. The prediction flow chart of the subsequent outage is shown in Fig. 6.

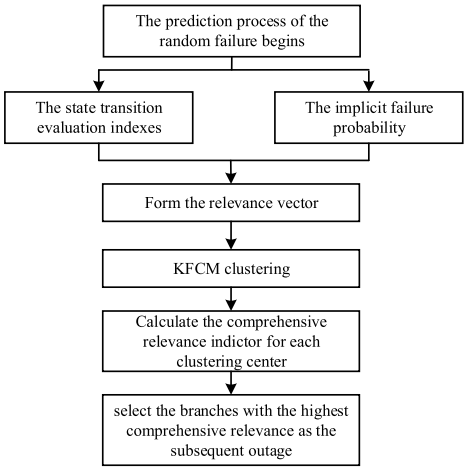

FIGURE 6. Prediction process of the random failure.

IV. COMPREHENSIVE ASSESSMENT ON CASCADING FAILURES

In order to effectively evaluate the impact severity of the fault chain, the comprehensive evaluation indictor is established in this paper, which consists of the total ratio of the load loss, the OEF dispatching cost ratio and the maximum operation connectivity.

The load loss of the cascading failure in IES is mainly determined to the effects of the energy island balancing and the load shedding control strategies. The thermal load loss ratio R_{hl} and the power load loss ratio R_{el} can be expressed as:

$$\begin{cases} R_{hl} = \dfrac{\sum_{i=1}^{S} (\Delta C_{h,i} + \Delta W_{h,i})}{SL_h} \\ R_{el} = \dfrac{\sum_{i=1}^{S} (\Delta C_{e,i} + \Delta W_{e,i})}{SL_e} \end{cases} \tag{28}$$

where S is the number of the branch outages in the fault chain. $\Delta C_{h,i}$ and $\Delta W_{h,i}$ represent the amount of thermal load shedding respectively during the heat island balancing process and the CHPC process. $\Delta C_{e,i}$ and $\Delta W_{e,i}$ represent the

amount of power load shedding respectively during the power island balancing and CHPC process after the i-th outage of the fault chain. L_h and L_e represent the total thermal demand and the total power demand.

The OEF dispatching cost ratio R_{OEF} can be calculated according to (29).

$$R_{OEF} = \frac{\sum_{i=1}^{S} Cost_{i,1}}{\sum_{i=1}^{S} Cost_{i,0}} \tag{29}$$

where $Cost_{i,0}$ and $Cost_{i,1}$ respectively represent the operation costs of IES before and after the performing of the control strategies.

The maximum operation connectivity R_G indicates the topological integrity of IES network, which can be calculated by (30):

$$R_G = \frac{\sum_{i=1}^{S} \left(N_{e,1}(i) + N_{h,1}(i)\right)}{S\left(N_{e,0} + N_{h,0}\right)} \tag{30}$$

where $N_{e,0}$ and $N_{h,0}$ respectively represent total number of the power lines and the total number of the pipelines. $N_{e,1}(i)$ is the maximum number of the power lines contained in the connected topology of the power network, and $N_{h,1}(i)$ is the maximum number of the pipelines contained in the connected topology of the heating network.

Based on the above indicators, the comprehensive evaluation index can be expressed as (31) to evaluate the impact severity of the fault chain. Note that the weight w_1, w_2 and w_3 in (31) can be determined by AHP algorithm [29].

$$R_C = \omega_1 \left(R_{hl} + R_{el}\right)/2 + \omega_2 R_{OEF} + \omega_3 / R_G \tag{31}$$

V. CASE STUDY AND DISCUSSIONS

A. CASE DESCRIPTION

In order to demonstrate the effectiveness of the proposed method, a case study was carried out in MATLAB. Fig. 7 shows the schematic of the testing case, which is supposed a self-sufficient IES, that is, isolated from external power system. The power network in the case has 14 bus bars, with one photovoltaic generator G2 connected to the node Bs2 and a thermal generator G1 connected to the node Bs6. The power load is 25.9 MW in total, and the basic parameters of the power lines and the generators are presented in Appendix, Table 7. The heating network has 17 nodes, including two heat source node of Bn6 and Bn7, 10 thermal load nodes and 5 main pipeline nodes. It was assumed that the initial supply temperature at each source is 90°C and the outlet temperature at each thermal load was set to fixed 30°C. The total heat power of all thermal loads is 21.4 MW, and other parameters of the heating network is listed in Appendix, Table 8. Note that the simulation model proposed in this paper is workable for different cases by adjusting the model parameters, and the model complexity is mainly determined by the scale of the IES.

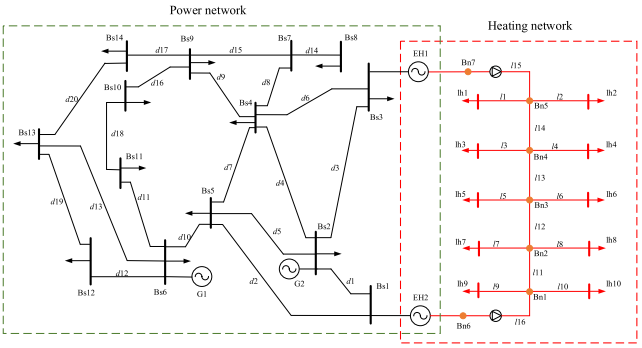

FIGURE 7. Schematic of the IES coupled heating and power network.

The power network and the heating network are interconnected through two EHs. The EH1, which is connected to the Bs3 node and the Bn7 node, is chosen as the heat slack node. The EH2, which is connected to the Bs1 node and Bn6 node, is chosen as the power slack node. Notice that two circulating pumps are set along the pipeline $l15$ and the pipeline $l16$, and the consumed power of the pumps, which is regarded as the power load, can be calculated according to [30]. What's more, the CHP unit contained in EH1 has a fixed thermoelectric ratio, and the CHP unit contained in EH2 has an adjustable thermoelectric ratio, which means the higher flexibility for dispatching. The structure of each EH is shown in Fig. 2.

B. RESULTS ANALYSIS AND DISCUSSIONS

1) ANALYSIS ON THE SIMULATION RESULTS OF CASCADING FAILURES

Calculate the initial risk of each branch according to (8) (9), and the calculation results are shown in Table 1. The top five branches with the highest risk value in the power network and the heating network are selected as the initial failures respectively, so as to form the initial fault sets of $\{d1, d10, d7, d13, d4, l16, l11, l15, l8, l12\}$.

TABLE 1. Initial risk of each branch.

Power line No.	Initial risk (10^{-4})	Pipeline No.	Initial risk (10^{-4})
***d*1**	**6.1655**	***l*16**	**56.0711**
***d*10**	**3.5700**	***l*11**	**18.9864**
***d*7**	**2.5047**	***l*15**	**15.5825**
d13	**1.8664**	***l*8**	**8.0980**
***d*4**	**0.8700**	***l*12**	**6.6965**
*d*8	0.8250	*l*14	4.5848
*d*14	0.8060	*l*5	3.7870
*d*11	0.7360	*l*6	3.1526
*d*2	0.7350	*l*7	1.9730
*d*20	0.5790	*l*3	1.5328
*d*18	0.2950	*l*9	1.3896
*d*6	0.2740	*l*4	1.3900
*d*15	0.2640	*l*10	1.3900
*d*3	0.2360	*l*2	0.8230
*d*9	0.09540	*l*1	0.7460
*d*12	0.0894	*l*13	0.1460
*d*5	0.0864		
*d*17	0.0156		
*d*16	0.0122		

Based on the simulation model of cascading failure proposed in this paper, 23 complete fault chains are obtained, including 13 of them corresponding to the initial failures in the power network and 10 of them corresponding to the initial failures in the heating network.

TABLE 2. Simulation results of the cascading failure.

No	Fault chain	Evaluation indictor of the cascading failure			
		R_{hl}/R_{el}	R_{OEF}	R_G	R_C
1	$d1\rightarrow d2$	0	0.771	0.972	0.599
2	$d1\rightarrow d10\rightarrow d15\rightarrow d9$	0	0.771	0.917	0.621
3	$d1\rightarrow d16\rightarrow d15\rightarrow d2$	0.079	0.924	0.986	0.673
4	$d10\rightarrow d1\rightarrow d9\rightarrow d11\rightarrow d13\rightarrow d12$	0.239	0.813	0.972	0.694
5	$d10\rightarrow d1\rightarrow d9\rightarrow d11\rightarrow d13\rightarrow d19$	0.215	0.813	0.968	0.687
6	$d10\rightarrow d1\rightarrow d9\rightarrow d11\rightarrow d17$	0.106	0.797	0.950	0.652
7	$d10\rightarrow d1\rightarrow d9\rightarrow d11\rightarrow d20$	0.163	0.797	0.956	0.669
8	$d10\rightarrow d1\rightarrow d9\rightarrow d2$	0	0.786	0.972	0.605
9	$d10\rightarrow d1\rightarrow d9\rightarrow d20\rightarrow d11$	0.163	0.789	0.956	0.667
10	$d10\rightarrow d1\rightarrow d15\rightarrow d9$	0.068	0.786	0.917	0.648
11	$d7\rightarrow d1\rightarrow d2$	0	0.791	0.972	0.606
12	$d13\rightarrow d19\rightarrow d20$	0	0	0.972	0.343
13	$d4\rightarrow d1\rightarrow d6\rightarrow d3$	0	0.770	0.972	0.599
14	$l16\rightarrow l13\rightarrow l14$	0.410	1	0.750	0.915
15	$l16\rightarrow l13\rightarrow l15$	**0.508**	**1**	**0.732**	**0.958**
16	$l11\rightarrow l13$	0.178	0.855	0.944	0.697
17	$l15\rightarrow d6\rightarrow d3$	0	0.212	0.972	0.413
18	$l15\rightarrow d3\rightarrow d6$	0	0.212	0.982	0.410
19	$l15\rightarrow l13\rightarrow l16$	0.452	0.212	0.630	0.751
20	$l12\rightarrow d1\rightarrow d2$	0	0.806	0.982	0.608
21	$l12\rightarrow d10\rightarrow d15\rightarrow d9$	0.027	0.806	0.898	0.649
22	$l12\rightarrow l16\rightarrow d1\rightarrow d2$	0.161	0.806	0.903	0.691
23	$l8\rightarrow l7\rightarrow l15$	0.017	1	0.963	0.685

Table 2 presents the simulation results of the cascading outage events for different initial outages. It is obvious that the fault chain "$d10 \rightarrow d1 \rightarrow d9 \rightarrow d11 \rightarrow d13 \rightarrow d12$" and "$d10 \rightarrow d1 \rightarrow d9 \rightarrow d11 \rightarrow d13 \rightarrow d19$" has the most outage branches, which contains three OEF dispatching processes with high dispatching costs. In addition, there exists power islands in these two fault chains, and due to the capacity restrictions of the power generation, part of the loads have been shed to ensure the power balance in the island. The fault chain "$d1 \rightarrow d2$" and "$l11 \rightarrow l13$" both contain only two outage branches. For the fault chain "$d1 \rightarrow d2$", the power generation of EH2 cannot be transmitted to other load nodes due to the disconnection of the power lines $d1$ and $d2$, leading to the formation of the power island. For the fault chain "$l11 \rightarrow l13$", the heat island is formed due to the outage of pipeline $l11$ and $l13$, resulting in 8.4 MW loss of thermal load. What's more, the fault chain with less outage branches may have worse evaluation indictors than the one with more outage branches, such as the fifth and sixteenth fault chain listed in Table 2, indicating that the number of the outage branches contained in a fault chain is not the only factor to determine the impact of the cascading failure. So it is necessary to establish effective evaluation indicators from multiple perspectives to achieve the comprehensive assessment of the impact of the cascading failure.

The fifteenth fault chain "$l16 \rightarrow l13 \rightarrow l15$" has the highest value of each evaluation indictor among all simulated fault chains, indicating the most serious impact it will have on the security of IES operation. The initial outage of the pipeline $l16$ caused the overload of the power line $l1$ and the pipelines $l14$, $l15$. As a result, the OEF dispatching strategy is firstly applied to responding to the overload. Then, 12.3% of the power and thermal load was lost due to the load shedding strategies in the condition that the OEF dispatching did not converge. After the last outage $l15$ of this fault chain, the two heat sources were disconnected from the heating network, leading to the interruption of the thermal load supply and the formation of the heat island.

What's more, during the simulation of the cascading failure, the initial outage in power network may cause the overload of the pipelines in the heating network, such as the overload of the pipeline $l16$ caused by the outage power lines "$d1 \rightarrow d16 \rightarrow d15$". Meanwhile, most overload in pipelines can be alleviated by the CHPC strategies. As a result, the outage branches of fault chains caused by the initial failure of the power network is mostly the power lines, which is corresponding to the results in Table2. Similar to the power network, the initial outage in the heating network may also cause the overload of the power lines. In this condition, the CHPC process is much more difficult, which leads to the failure of the co-controlling more easily, so the fault chains caused by the initial failure in the heating network usually contains both pipeline outages and power line outages.

In order to further verify the superiority of the model proposed in this paper, three cases with different analysis methods of the cascading failure are designed as follows:

Case I: Without considering the CHPC strategies, which means that if the overload occurs in one branch, the corresponding branch will be removed directly.

Case II: Without considering the clustering during the prediction process of the random failures, which means that only the branch with the highest value of relevance will be chosen as the subsequent outage.

Case III: Simulate the cascading failure with the complete method proposed in this paper.

Fig. 8 shows the occurrence frequency of each branch in all simulated fault chains. In Case III, power line $d1$ has the highest occurrence frequency in all fault chains listed in Table 2, and the power line $d10$, $d9$ and $d11$ also appear in the simulated fault chains many times. Most of these power lines with high occurrence frequency are the critical link lines of the power network, which play important roles in the power transmission and interaction between different areas. Once the failure occurs in one of them, the power flow will transfer to other power lines, leading to the overload of other branches, so as to cause the cascading failure.

TABLE 3. The top three branches with the highest occurrence frequency.

Case \ Order	1		2		3	
	Branch No.	Frequency	Branch No.	Frequency	Branch No.	Frequency
Case III	***d*1**	15.85%	*d*10/*d*9	9.76%	***l*15**/*d*11	6.1%
Case II	***d*1**	16.67%	***l*15**/*d*2	10%	*l*13/*d*6	6.67%
Case I	***d*1**/*d*2	24.14%	***l*15**	13.79%	*l*16	6.9%

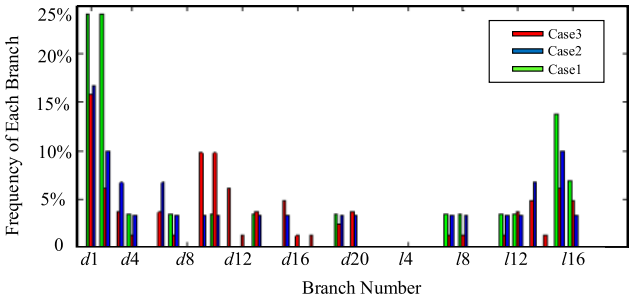

FIGURE 8. The occurrence frequency of each branch in all simulated fault chains.

Table 3 listed the top three branches with the highest occurrence frequency in the simulated fault chains in case I, II and III. According to the statistical results, we can find that both the power line $d1$ and the pipeline $l15$ have high occurrence frequency in three cases, indicating that these two branches can be regarded as the vulnerable component of the IES network which play important roles in promoting the development of the cascading failure. So, some improvement measures can be designed for the vulnerable branches to prevent cascading outages.

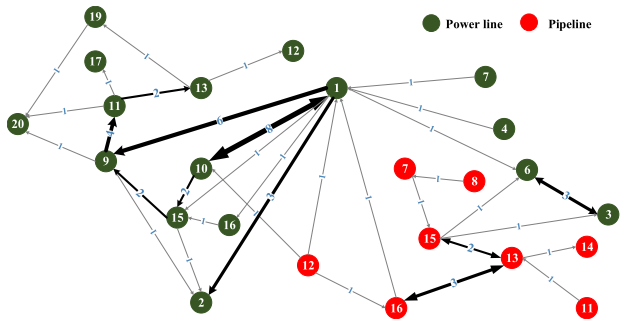

FIGURE 9. Relevance network diagram of cascading failure branches.

Fig. 9 shows the relevance network diagram of cascading failure branches. In Fig. 9, each node represents the corresponding power line number or the pipeline number, the connection and direction between nodes represent the interactions between outage branches, and the thickness of the connection line means the strength of their interactions. What's more, the interaction usually exists between two adjacent outage events in the fault chain, and the interaction strength is determined to the number of the fault chain containing these two adjacent outage branches. The bigger the number is, the stronger interaction, as well as the correlation between them will be.

As shown in Fig. 9, it is obvious that the correlation between the power line $d1$ and $d10$ is the highest among all the branches, which indicates the strong bidirectional interaction between them. What's more, we can find that the branches with the strong correlation mainly exist in the same energy system, and there rarely exists the strong-correlated branches in two different energy systems due to the combined heat and power control strategies, which indicates that the control strategies play an important role in adjusting the operation sate of IES and blocking the development of the cascading failure. In conclusion, the method proposed in this paper can be used to locate the vulnerable components and search subsequent outages in order to stop cascading outage spreading.

2) COMPARISON OF THE EFFECTS ON SIMULATION RESULTS IN DIFFERENT CASES

In this section, the cascading outage events corresponding to the initial outage of the power line $d10$ and the pipeline $l12$ are selected respectively as the examples for further analysis.

TABLE 4. Simulation results in different cases for the initial outage of ***d*10**.

Case	Fault chain	R_{hl}/R_{el}	R_{OEF}	R_G
I	$d10\rightarrow d1\rightarrow d2$	0	0	0.972
II	$d10\rightarrow d1\rightarrow d15\rightarrow d9$	0	0.785	0.917
III	$d10\rightarrow d1\rightarrow d9\rightarrow d11\rightarrow d1\rightarrow d12$	0.239	0.813	0.972
III	$d10\rightarrow d1\rightarrow d9\rightarrow d11\rightarrow d13\rightarrow d19$	0.215	0.813	0.968
III	$d10\rightarrow d1\rightarrow d9\rightarrow d11\rightarrow d\ 17$	0.106	0.797	0.950
III	$d10\rightarrow d1\rightarrow d9\rightarrow d11\rightarrow d\ 20$	0.163	0.797	0.956
III	$d10\rightarrow d1\rightarrow d9\rightarrow d2$	0	0.786	0.972
III	$d10\rightarrow d1\rightarrow d9\rightarrow d20\rightarrow d11$	0.163	0.789	0.956
III	$d10\rightarrow d1\rightarrow d15\rightarrow d9$	0.068	0.786	0.917

TABLE 5. Simulation results in different cases for the initial outage of ***l*12**.

Case	Fault chain	R_{hl}/R_{el}	R_{OEF}	R_G
I	$l12\rightarrow d1\rightarrow d2$	0	0.806	0.982
II	$l12\rightarrow d1\rightarrow d2$	0	0.806	0.982
III	$l12\rightarrow d1\rightarrow d2$	0	0.806	0.982
III	$l12\rightarrow d10\rightarrow d15\rightarrow d9$	0.027	0.806	0.898
III	$l12\rightarrow l16\rightarrow d1\rightarrow d2$	0.161	0.806	0.903

Table 4 and Table 5 present the simulation results in different cases for the initial outage of $d10$ and $l12$. For case III, there exists seven development modes of the cascading failure for the initial outage of $d10$. While for case II, only one

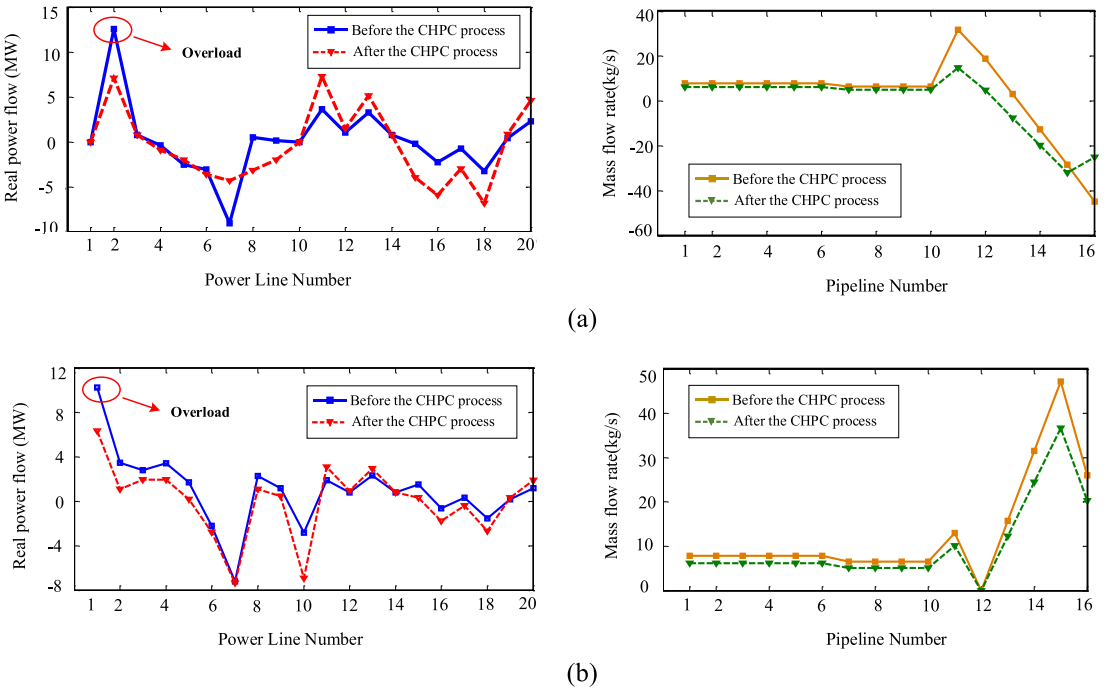

FIGURE 10. (a) The distribution of power flow and mass flow rate for the initial outage of $d10$. (b) The distribution of the power flow and mass flow rate for the initial outage of $l12$.

branch with the highest comprehensive relevance will be chosen as the subsequent outage without the clustering process. As a result, only one fault chain "$d10 \rightarrow d1 \rightarrow d15 \rightarrow d9$" has been searched, resulting in the ignorance of other important outages related to the power line $d9$. Similar to the initial outage of $d10$, three fault chains corresponding to the initial outage of the pipeline $l12$ are obtained with the co-controlling strategies and the clustering method, while for the case II, only one fault chain "$l12 \rightarrow d1 \rightarrow d2$" has been searched. So, in order to search more comprehensive development modes of the cascading failure, the clustering method can be taken into account during the prediction process of the random failure.

Fig. 10 presents the power flow and mass flow rate distribution corresponding to the initial outage of $d10$ and $l12$ during their first CHPC process. It is obvious that by using the CHPC strategies, the overload branches, such the power line $d1$ and $d2$, are operating in the new security condition with the overload pressure of the branch alleviated. While in case I, without taking the CHPC strategies into account, only one fault chain "$d10 \rightarrow d1 \rightarrow d2$" will be formed for the initial outage of $d10$, as well as the fault chain "$l12 \rightarrow d1 \rightarrow d2$" corresponding to the initial outage of $l12$, which indicates that the CHPC strategies play an important role in the development of the cascading failure, and the simulation model considering CHPC strategies in this paper is of effectiveness and rationality.

3) ANALYSIS OF THE IMPACT OF LOAD LEVELS ON THE CASCADING FAILURE

During the searching process of the fault chain, the power loads or thermal loads at each node are considered invariable.

TABLE 6. Simulation results of the fault chain with different load levels.

Load level	Fault chain	R_{hl}/R_{el}	R_{OEF}	R_G	R_C
Peak load level	$d10 \rightarrow d11 \rightarrow d13 \rightarrow d12$	0.342	1.109	0.972	0.827
	$d10 \rightarrow d11 \rightarrow d13 \rightarrow d19$	0.318	1.109	0.965	0.821
	$d10 \rightarrow d11 \rightarrow d20$	0.266	1.092	0.944	0.806
	$d10 \rightarrow d16 \rightarrow d20$	0.218	1.081	0.926	0.793
	$d10 \rightarrow d16 \rightarrow d13 \rightarrow d12$	0.342	1.105	0.958	0.830
	$d10 \rightarrow d16 \rightarrow d13 \rightarrow d19$	0.318	1.105	0.951	0.825
	$d10 \rightarrow d16 \rightarrow d11$	0.048	1.081	0.963	0.723
	$d10 \rightarrow d20 \rightarrow d11$	0.266	1.085	0.944	0.803
Flat load level	$d10 \rightarrow d16 \rightarrow d13 \rightarrow d12$	0	0.236	0.926	0.439
	$d10 \rightarrow d16 \rightarrow d13 \rightarrow d12$	0.026	0	0.958	0.357
	$d10 \rightarrow d16 \rightarrow d17 \rightarrow d19$	0	0	0.938	0.355
	$d10 \rightarrow l13 \rightarrow l11$	0.355	0	0.926	0.478
Valley load level	$d10 \rightarrow l13 \rightarrow d1 \rightarrow d2$	0.0347	0.792	0.972	0.817
	$d10 \rightarrow d1 \rightarrow d2$	0	0	0.972	0.343
	$d10 \rightarrow d7 \rightarrow d11 \rightarrow d17$	0.0757	0	0.944	0.379
	$d10 \rightarrow d7 \rightarrow d11 \rightarrow d20$	0.0757	0	0.951	0.376
	$d10 \rightarrow d7 \rightarrow d15 \rightarrow d9$	0	0.631	0.917	0.573

In order to further analyze the impact of load levels on the development of the cascading failure in IES, three different load levels: peak load level, valley load level and flat load level are designed for the simulation of the cascading failure. Note that the peak load is set as the 1.2 times of the current load demand, the valley load is set as the 30% of the current load demand, and the flat load is set as the 60% of the current load demand.

We take the fault chain corresponding to the initial outage of $d10$ as an example, and searched fault chains with different load levels. As can be seen from the simulation results listed in Table 6, eight fault chains are formed in case of the peak

load level with the higher comprehensive evaluation indictor than the current load level, and in case of the valley and flat load level, only four and five fault chains are obtained with the lower comprehensive evaluation indictors than the current load level. In the peak load demand period, the power flow and mass flow rates in branches increased significantly, leading to the high costs for coordinated controlling. While in the valley or flat load demand period, the load rate of each branch is relatively low, leading to the low costs for coordinated controlling and the smaller scale of the cascading failure.

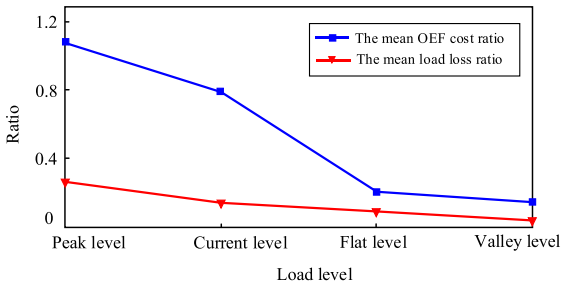

FIGURE 11. The mean load loss ratio and mean OEF cost ratio of the fault chains with different load levels.

As shown in Fig. 11, the load loss ratio and OEF dispatching cost ratio of the cascading failure increase gradually with the increase of the load level, which indicates that the load level has a great impact on the scale and seriousness of the cascading failure. Meanwhile, serious and large-scale cascading failures are more likely to occur in case of high load demand, so it is necessary to pay more attention to preventing the occurrence and spreading of the cascading failure during the peak load period.

VI. CONCLUSION

In order to deeply analyze the propagation mechanism of the cascading failure in IES, a novel simulation model of the cascading failure considering the interaction between the coupled heating and power networks is proposed in this paper. According to the simulation results of the case study, main conclusions are listed as follows:

1) The transmission process of the IES cascading failure is mostly bidirectional due to the deep coupling of the heating and power systems. The vulnerable components usually can be located to the key link lines and the main energy-supply branches, which promote the transitions of the energy flow and overload in other branches.

2) Compared with traditional simulation methods of the cascading failure, the proposed model in this paper can significantly improve the overload conditions by considering the CHPC strategies, which conforms to the actual operation and dispatching process of IES, ensuring the rationality and effectiveness of the predicted fault chains.

3) The combination of the state transition evaluation indictor and the implicit failure probability indictor can effectively describe the relevance between the initial failure and its subsequent failures. What's more, by applying the clustering method and choosing the sets of branches with higher relevance indictors during the prediction process of the random failure, the more comprehensive development modes of the cascading failure can be searched.

4) The load level has a great impact on the scale and seriousness of the cascading failure, serious and large-scale cascading failures are more likely to occur in case of high load demand, which relies on the effective measures to prevent the occurrence and spreading of the cascading failure.

APPENDIX

See Tables 7 and 8.

TABLE 7. Basic parameters of the power network.

Power line no.	Line impedance (pu)	Power flow limitation (MW)	Bus bar no.	Power load(MW)
$d1$	0.019+j0.059	10	Bs1	0
$d2$	0.054+j0.223	10	Bs2	2.17
$d3$	0.047+j0.198	8	Bs3	8.62
$d4$	0.058+0.176	8	Bs4	4.78
$d5$	0.057+0.174	8	Bs5	0.76
$d6$	0.067+j0.171	10	Bs6	1.12
$d7$	0.013+j0.042	10	Bs7	0
$d8$	j0.209	6	Bs8	0.80
$d9$	j0.556	6	Bs9	2.95
$d10$	j0.252	10	Bs10	0.90
$d11$	0.095+j0.199	10	Bs11	0.35
$d12$	0.123+j0.256	10	Bs12	0.61
$d13$	0.066+j0.130	10	Bs13	1.35
$d14$	0.000+j0.176	8	Bs14	1.49
$d15$	0.000+j0.110	8		
$d16$	0.032+j0.085	6		
$d17$	0.127+j0.270	6		
$d18$	0.082+j0.192	8		
$d19$	0.221+j0.200	8		
$d20$	0.171+j0.348	8		

TABLE 8. Basic parameters of the heating network.

Pipe no.	Pipe length(m)	Heat transfer coefficient	Thermal load (MW)	Mass flow rate limitation(kg/s)
$l1$	95.20	0.189	2.3	10
$l2$	105.10	0.189	2.3	10
$l3$	136.00	0.189	2.3	10
$l4$	123.30	0.189	2.3	10
$l5$	161.10	0.189	2.3	10
$l6$	134.20	0.189	2.3	10
$l7$	136.40	0.189	1.9	10
$l8$	134.10	0.189	1.9	10
$l9$	136.40	0.189	1.9	10
$l10$	136.20	0.189	1.9	10
$l11$	61.80	0.219	-	60
$l12$	64.90	0.278	-	40
$l13$	61.70	0.236	-	40
$l14$	72.10	0.236	-	40
$l15$	81.80	0.210	-	40
$l16$	90.60	0.321	-	60

REFERENCES

[1] E. Widl, T. Jacobs, D. Schwabeneder, S. Nicolas, D. Basciotti, S. Henein, T. G. Noh, O. Terreros, A. Schuelke, and H. Auer, "Studying the potential of multi-carrier energy distribution grids: A holistic approach," *Energy*, vol. 153, pp. 519–529, Jun. 2018.

[2] J. Li, J. Fang, Q. Zeng, and Z. Chen, "Optimal operation of the integrated electrical and heating systems to accommodate the intermittent renewable sources," *Appl. Energy*, vol. 167, pp. 244–254, Apr. 2016.
[3] X. Zhang, M. Shahidehpour, A. Alabdulwahab, and A. Abusorrah, "Optimal expansion planning of energy hub with multiple energy infrastructures," *IEEE Trans. Smart Grid*, vol. 6, no. 5, pp. 2302–2311, Sep. 2015.
[4] M. Chertkov, S. Backhaus, and V. Lebedev, "Cascading of fluctuations in interdependent energy infrastructures: Gas-grid coupling," *Appl. Energy*, vol. 160, pp. 541–551, Dec. 2015.
[5] Z. Qiao, Q. Guo, H. Sun, Z. Pan, Y. Liu, and W. Xiong, "An interval gas flow analysis in natural gas and electricity coupled networks considering the uncertainty of wind power," *Appl. Energy*, vol. 201, pp. 343–353, Sep. 2017.
[6] C. Yan, C. Wang, and C. X. Wang, "Risk-based methods for sustainable energy system planning: A review," *Power Syst. Technol.*, vol. 43, pp. 12–22, Jan. 2019.
[7] N. Gholizadeh, M. J. Vahid-Pakdel, and B. Mohammadi-Ivatlo, "Enhancement of demand supply's security using power to gas technology in networked energy hubs," *Int. J. Electr. Power Energy Syst.*, vol. 43, pp. 83–94, Jul. 2019.
[8] M. Ding, Y. Xiao, J. J. Zhang, and J. He, "Risk assessment model of power grid cascading failures based on fault chain and dynamic fault tree," *Proc. CSEE*, vol. 35, Feb. 2015, pp. 821–829.
[9] R. Yao, S. Huang, K. Sun, F. Liu, X. Zhang, S. Mei, W. Wei, and L. Ding, "Risk assessment of multi-timescale cascading outages based on Markovian tree search," *IEEE Trans. Power Syst.*, vol. 32, no. 4, pp. 2887–2900, Jul. 2017.
[10] J. Qi, I. Dobson, and S. Mei, "Towards estimating the statistics of simulated cascades of outages with branching processes," *IEEE Trans. Power Syst.*, vol. 28, no. 3, pp. 3410–3419, Aug. 2013.
[11] M. L. Bao, "Assessment of cascading failures in power system considering the effects of natural gas system," *Power Syst. Technol.*, vol. 43, no. 1, pp. 32–40, Jan. 2019.
[12] Z. G. Pan, Q. L. Guo, and H. B. Sun, "Interactions of district electricity and heating systems considering time-scale characteristics based on quasi-steady multi-energy flow," *Appl. Energy*, vol. 167, pp. 230–243, Apr. 2016.
[13] J. Yu, L. Guo, M. Ma, S. Kamel, W. Li, and X. Song, "Risk assessment of integrated electrical, natural gas and district heating systems considering solar thermal CHP plants and electric boilers," *Int. J. Electr. Power Energy Syst.*, vol. 103, pp. 277–287, Dec. 2018.
[14] X. Liu, J. Wu, N. Jenkins, and A. Bagdanavicius, "Combined analysis of electricity and heat networks," *Appl. Energy*, vol. 162, pp. 1238–1250, Jan. 2016.
[15] J. F. Zheng, Z. G. Zhou, J. N. Zhao, and J. D. Wang, "Integrated heat and power dispatch truly utilizing thermal inertia of district heating network for wind power integration," *Appl. Energy*, vol. 211, pp. 865–874, Feb. 2018.
[16] S. V. Buldyrev, R. Parshani, G. Paul, H. E. Stanley, and S. Havlin, "Catastrophic cascade of failures in interdependent networks," *Nature*, vol. 464, pp. 1025–1028, Apr. 2010.
[17] B. F. Luo, "Static sensitivity analysis of integrated electricity and gas system based on unified power flow model," *Automat. Electr. Power Syst.*, vol. 42, no. 13, pp. 29–35, 2016.
[18] X. Q. Fu, Q. Guo, H. Sun, X. Zhang, and L. Wang, "Estimation of the failure probability of an integrated energy system based on the first order reliability method," *Energy*, vol. 134, pp. 1068–1078, Sep. 2017.
[19] E. Guelpa and V. Verda, "Model for optimal malfunction management in extended district heating networks," *Appl. Energy*, vol. 230, pp. 519–530, Nov. 2018.
[20] J. C. Mei, "Hybrid control of integrated power and gas energy systems based on significant contingency screening," *Power Syst. Technol.*, vol. 43, no. 1, pp. 23–31, Jan. 2019.
[21] M. Badami, A. Fonti, A. Carpignano, and D. Grosso, "Design of district heating networks through an integrated thermo-fluid dynamics and reliability modelling approach," *Energy*, vol. 144, pp. 826–838, Feb. 2018.
[22] S. Chen, Z. Wei, G. Sun, K. W. Cheung, D. Wang, and H. Zang, "Adaptive robust day-ahead dispatch for urban energy systems," *IEEE Trans. Ind. Electron.*, vol. 66, no. 2, pp. 1379–1390, Feb. 2019.
[23] B. Park and C. L. DeMarco, "Convex relaxation of sparse tableau formulation for the AC optimal power flow," *Electr. Power Syst. Res.*, vol. 171, pp. 209–218, Jun. 2019.
[24] E. D. Liu and P. Cheng, "Mitigating cyber privacy leakage for distributed DC optimal power flow in smart grid with radial topology," *IEEE Access*, vol. 6, pp. 7911–7920, 2018.
[25] L. Zhang, Y. Luo, H. Luo, S. Miao, J. Ye, G. Zhou, and L. Sun, "Scheduling of integrated heat and power system considering multipletime-scale flexibility of CHP unit based on heat characteristic of DHS," *Proc. CSEE*, vol. 38, no. 4, pp. 985–998, Feb. 2018.
[26] S. X. Liu, "Power flow model and algorithm of combined power and heat system considering heat loss in returen pipe network," *Autom. Electr. Power Syst.*, vol. 42, no. 4, pp. 77–81, Feb. 2018.
[27] D. E. Newman, B. A. Carreras, V. E. Lynch, and I. Dobson, "Exploring complex systems aspects of blackout risk and mitigation," *IEEE Trans. Rel.*, vol. 60, no. 1, pp. 134–143, Mar. 2011.
[28] P. Henneaux, P. E. Labeau, J. C. Maun, and L. Haarla, "A two-level probabilistic risk assessment of cascading outages," *IEEE Trans. Power Syst.*, vol. 31, no. 3, pp. 2393–2403, May 2016.
[29] J. Benitez, S. Carpitella, A. Certa, and J. Izquierdo, "Management of uncertain pairwise comparisons in AHP through probabilistic concepts," *Appl. Soft Comput.*, vol. 78, pp. 274–285, May 2019.
[30] Z. B. Yang, "A decoupling method for energy flow calculation of microgrids with combined cooling, heating and power," *Power Syst. Technol.*, vol. 41, pp. 3876–3883, Jul. 2017.

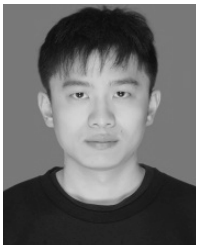

YI PAN received the B.S. degree in electrical engineering from Southwest Jiaotong University, Chengdu, China, in 2015. He is currently pursing the Ph.D. degree in electrical engineering with Southeast University, Nanjing, China. His research interests include integrated energy system optimal operation, power system fault diagnosis, and signal processing.

FEI MEI received the Ph.D. degree in electrical engineering from Southeast University, in 2014. He is currently a Lecturer with the College of Energy and Electrical Engineering, Hohai University. His research interests include smart grid, online monitoring, and signal processing.

CHENG ZHOU received the B.S. degree in electrical engineering from the Nanjing Institute of Technology, Nanjing, China. She is currently pursuing the M.S. degree in electrical engineering with Southeast University, Nanjing. Her research interests include the simulation of power systems and the optimization of the integrated energy systems.

TIAN SHI received the B.S. degree in electrical engineering from the Nanjing Institute of Technology, Nanjing, China. He is currently pursuing the M.S. degree in electrical engineering with Southeast University, Nanjing. His research interests include smart grid and power system load forecasting.

JIANYONG ZHENG received the Ph.D. degree from the School of Electrical Engineering, Southeast University, China, in 1999, where he is currently a Full Professor. His research interests include the application of power electronics device, power system automation, and renewable energy technology.